CONTROL STRATEGY FOR MEASUREMENT PERFORMANCE ENHANCEMENT OF A MICROMACHINED ACCELEROMETER

Jonathan Soen [*,**] **Alina Voda** [**] and **Cyril Condemine** [*]

[*] *Laboratory of Electronics and Information Technologies (CEA-LETI-DCIS), 17 rue des Martyrs, 38054 Grenoble, France*

[**] *Automatic Control Laboratory of Grenoble (LAG), ENSIEG-INPG, BP 46, 38402 Saint Martin d'Hères, France*

Abstract: This paper presents the design of a closed-loop micromachined accelerometer using a sensitivity functions shaping approach in order to reach the desired measurement performance. The controller design is based on an identified model of the plant (MEMS, readout circuit and actuator) and a pole placement strategy. Simulation results and real-time application on a prototype show the feasibility and the interest of this methodology for high performance microsystem design.

Keywords: Closed-loop systems, Sensors, Microsystems, Accelerometers, Control system design, Pole assignment, Sensitivity functions shaping.

1. INTRODUCTION

Microsystems are dynamic systems which often contain feedback. Their design and their usage rise problems which can be solved by automatic control although, at present time, this is not systematically done. The specificities of those microsystems, their small dimensions, the resulting physical phenomena and the high electronic integration, call for a very thorough study if we want to apply control strategies (identification, observation, feedback control). Indeed, microsystems can include non-linearities, couplings, various noise sources. Moreover, the dynamics of their electronics, which can often be neglected in macrosystems, can play an important role concerning the achievable performance. Therefore, these systems necessitate a detailed preliminary analysis to translate the existing physical schemes into (virtual) ones suitable for control design.

Most of the commercial accelerometers operate in open loop. However, closed-loop accelerometers appear as their performance (linearity, sensitivity, noise rejection) can be higher than the open-loop ones (Chau *et al.* 1996, Kraft 2000, Lemkin *et al.* 1997). This paper presents feedback control strategy applied to the design of a high performance closed-loop micromachined accelerometer.

Section 2 presents the system overview and the problem statement. The control strategy is described in section 3. Simulation results and the prototype performance are given in sections 4 and 5.

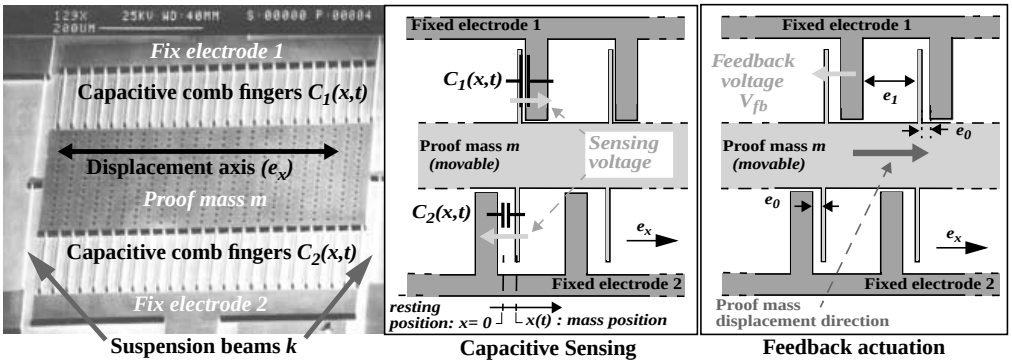

Fig. 1. Scanning Electron Microscope view of the capacitive accelerometer MEMS and detailed schematics

2. SYSTEM OVERVIEW AND PROBLEM STATEMENT

2.1 Sensing element and measurement/actuation principle

The micromachined accelerometer (fig. 1) is fabricated on a SOI substrate. It is composed of a movable proof mass m maintained in its rest position ($x = 0$) by two suspension beams. Two variable sense capacitances $C_1(x,t)$ and $C_2(x,t)$ are obtained between the interdigitated comb fingers of the fixed electrodes and those of the movable proof mass m. This capacitive interface will be used both as the sensing element and the feedback actuator. Indeed, under an external acceleration $\gamma(t)$, inertial forces act on the movable proof mass m. Its displacement $x(t)$ is proportional to the external acceleration $\gamma(t)$ for low frequencies. This displacement translates into a variation of capacitance $\Delta C(x,t)$, proportional to $C_1(x,t)$-$C_2(x,t)$, which can be measured by an appropriate sensing and pickup circuit. Applying a potential difference V_{fb} between the fixed electrode 1 and the movable proof mass will create an attractive electrostatic force and the proof mass m will move towards the right (fig. 1) (respectively towards the left if V_{fb} is applied between electrode 2 and the proof mass). In closed-loop operation, capacitance readout and feedback actuation will be performed through $\Sigma\Delta$ interfaces. They carry out a direct analog capacitance to digital word conversion (readout ADC) and a digital word to electrostatic forces conversion (feedback actuation DAC) with reduced analog electronics (Delorme *et al.* 2003).

Table 1. Desired performance

Characteristic	Requirements
Measurement Full Scale (FS)	$\gamma_{max} = \pm\ 10\ g$
Meas. BandWidth (MBW)	$0 - 122\ Hz$
Measurement Accuracy	$\lvert\varepsilon_m(t)/\gamma(t)\rvert \leq -100\ dB$
Measurement Linearity	$THD \leq -100\ dB$
Digital Resolution	$SQNR \geq 100\ dB$
Resulting $SNDR$	$SNDR \geq 100\ dB$
Temperature Range	$0 - 85°C$
Pressure Range	$0.8 - 1.2\ atm$

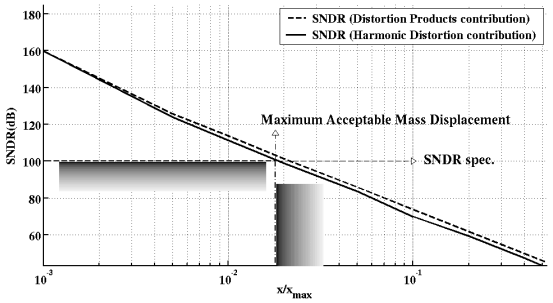

Fig. 2. Achievable SNDR versus amplitude of mass displacement x: Harmonic Distortion contribution (solid line) and Distortion products contribution (dashed line).

2.2 Capacitive sensing nonlinearities

The nonlinearity of the capacitive sensing interface introduces distortions in the measurement signal. These distortions dramatically affect the measurement Signal to Noise and Distortion Ratio (SNDR). Reducing those effects will be the main goal of this closed-loop design. Considering figure 2, it can be inferred that, in order to comply with the system specification for SNDR (table 1), the mass displacement should be kept smaller than 2% of the mass maximum open-loop displacement x_{max}. This can be achieved by an appropriate feedback controller design.

2.3 Technological dispersion and design choices

Since MEMS fabrication is subject to technological dispersions, a model based on the discretization of the nominal physical model of the system may lead to a non-robust design. Indeed, especially in the prototyping step, the designed mechanical part and the fabricated one could be (slightly) different, so that the mass and the mechanical stiffness can be modified as well as the interdigitated capacitance gap and consequently the readout gain, the actuation gain and the effective natural frequency. In order to draw aside this problem of robustness towards parameter value mismatch, the microsystem's

Integrated Circuit has been designed in order to allow the identification of the *plant to be controlled*. This identification will provide a discrete-time model of the whole plant, including the dynamics of the mechanical part, those of the ADC and DAC [1], as well as the effects of the readout and the actuation on the mass dynamics. For flexibility purpose, it has been chosen to implement a RS-type digital controller whose coefficients can be uploaded into the memory of the digital part of the specific Integrated Circuit.

3. CONTROL STRATEGY

3.1 Block diagram of the closed loop measurement system

The closed-loop architecture resulting from the previous considerations is given in figure 3a. In order to separate the controller and the plant to be controlled, this schematic is modified according to figure 3b, by rotating the diagram blocks. This physical system can now be modelled as a standard (virtual) feedback loop with *linear* transfers (fig. 3c). This representation is valid since the mass displacement $x(t)$ is kept small by feedback. In this schematic, all signals are normalized. Some of the transfer functions are considered to be known ($G_{d_0}(q^{-1})$, $G_{d_1}(q^{-1})$ & $G_{d_2}(q^{-1})$), whereas the plant transfer function $G(q^{-1})$ will be obtained by identification (*cf.* subsection 3.3).

3.2 Physical plant model

Although real plant model $G(q^{-}1)$ will be obtained by identification, a physical model is required for validation purpose. The system dynamics is mainly represented by a classical damped mass-spring system, in which the mass is the proof mass m and the damping coefficient $b(x,T,t)$, due to air viscosity, is nonlinear and temperature dependant. The spring coefficient k_{eff} results from a combined action of the suspension beam mechanical stiffness and the electrostatic softening stiffness (Handtmann *et al.* 2002). The resulting approximate mass motion equation is finally given by:

$$m.\ddot{x}(t) + b(x,T,t).\dot{x}(t) + k_{eff}.x(t) = ... \\ = m.g.\gamma(t) + K_u.u(k) \quad (1)$$

[1] $\Sigma\Delta$ ADC and DAC of figure 3 include digital down/up sampling filters in order to adapt the relatively low frequency required for identification and control purpose ($f_s = 62.5kHz$) to the high frequency (250 kHz) required for quantization noise shaping (Norsworthy *et al.* 1996).

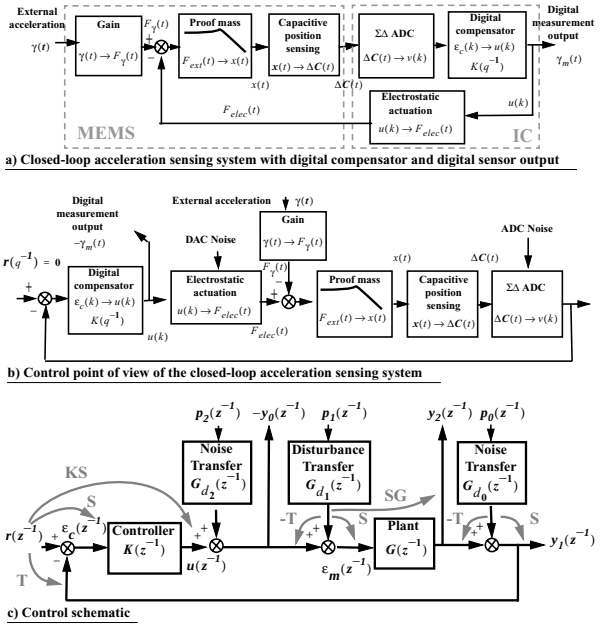

Fig. 3. a) Closed-loop sensing schematic. b) Modified schematic. c) Control schematic

where $\gamma(t)$ the external acceleration, $u(k)$ the sampled control signal and K_u the actuation gain. Considering the linearized value b_{lin} of $b(x,T,t)$ around the rest position ($x = 0$) at ambient temperature $T = 300K$, an approximate transfer function from the control signal $u(k)$ to the mass displacement $x(t)$ can be proposed (2).

$$G_{th}(s) = \frac{X(s)}{U^*(s)} = \frac{K_u}{m.s^2 + b_{lin}.s + k_{eff}} \quad (2)$$

where $U^*(s)$ is the starred Laplace transform of $u(k)$.

3.3 Identified plant model (simulation)

The identification of the plant's transfer function $G(z^{-1})$ is performed in open loop between input $u(k)$ and output $y_1(k)$ (fig. 3c), where $y_1(k)$ is the image of the mass position $x(t)$ through the capacitive position sensing element. The excitation signal proposed for identification is a PRBS signal. Using the Matlab® Identification Toolbox, the best fit was obtained with a 4^{th} order ARMAX model which is in good accordance with the physical model G_{th} (2) multiplied by the capacitance readout gain K_{LC} (fig. 4).

3.4 Performance and stability robustness

Using the control block diagram (fig. 3c), stability and performance requirements can easily be expressed by means of templates on the closed loop sensitivity functions **K**, **S**, **KS** and **SG** (Landau and Karimi 1998) (*cf.* arrows on fig. 3c).

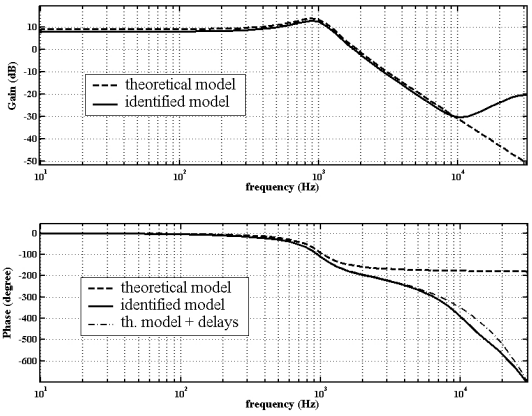

Fig. 4. Bode diagram of the identified transfer $G(z^{-1})$ (solid line) and of the theoretical model $K_{LC}.G_{th}$(dashed line). The dashed dot line represents theoretical model phase fit adding 1 sampled delay at f_s.

In order to ensure sufficient *stability margins* (Skogestad and Postlethwaite 1996), the maximum $\|\mathbf{S}\|_\infty$ of the sensitivity function $\mathbf{S}$ should be inferior to 6 dB (3). The related graphical template is denoted *Template 1* on figure 5. In the same manner, the complementary sensitivity function maximum $\|\mathbf{T}\|_\infty$ should be inferior to 3.5 dB (4) - *Template 2. Template 3* on the sensitivity $\mathbf{KS}$ (5) is added to prevent instability due to saturation effects in the electronic part - numerical computation overflow in the implemented digital controller $K(z^{-1})$.

$$\|T_{\varepsilon_c r}(z^{-1})\|_\infty = \|\mathbf{S}(z^{-1})\|_\infty \leq 6\ dB \quad (3)$$

$$\|T_{y_1 r}(z^{-1})\|_\infty = \|\mathbf{T}(z^{-1})\|_\infty \leq 3.5\ dB \quad (4)$$

$$\|T_{up}(z^{-1})\|_\infty = \|\mathbf{KS}(z^{-1})\|_\infty \leq 15\ dB \quad (5)$$

Nominal (measurement) performance can also be expressed by means of templates. For instance, the measurement accuracy - relative measurement error in table 1- is equal to the ratio between the magnitude of the measurement error signal $|-\varepsilon_m(k)| = |y_0(k) - p_1(k)|$ and the magnitude of the (normalized) external acceleration $|p_1(k)|$. This ratio depends on the input frequency and can be associated to the transfer function $T_{\varepsilon_m p_1}(z^{-1})$. Considering figure 3c and table 1, the relation (6)[2] can be written, which is equivalent to *Template 5* on the $\mathbf{S}$ sensitivity function plot (fig. 5).

$$|T_{\varepsilon_m p_1}(z^{-1})| = |\mathbf{S}.G_{d_1}(z^{-1})| \leq -100\ dB\ in\ MBW$$
$$\Rightarrow |\mathbf{S}(z^{-1})| \leq -100\ dB\ in\ MBW \quad (6)$$

In the same manner, other templates (not detailed here) should be fulfilled such as:
- *Template 4* to ensure measurement bandwidth;
- *Template 6* for measurement linearity;
- *Template 9* for analog to digital conversion resolution;
- *Template 10* for *stability robustness* towards parameter variation (temperature varying damping coefficient $b(x,T,t)$) (Doyle *et al.* 1992).

In order to characterize *performance robustness*, it will be verified *a posteriori* if the sensitivity functions identified on the perturbed system (worst case parameter variation: $b_{lin} \pm 15\%$) still fulfil the performance templates.

4. SIMULATION RESULTS

The controller has been designed using the pole placement with sensitivity function shaping method (Landau and Karimi 1998). This method has several advantages. It provides an instantaneous view of expectable sensor and control loop performance in terms of sensitivity functions, so that the compromise between stability and measurement performance can be realized. Furthermore, the designer fixes the controller order by choosing the fixed polynomials degrees, so that no controller order reduction method has to be applied *a posteriori*. In this study, the maximum order of the controller is imposed by the electronics. It must be lower than 8.

4.1 Control-loop performance

The following results have been obtained for a controller designed in order to closely comply with the *nominal (measurement) performance* specifications (table 1 and related templates). As a consequence, stability margins are a bit weak. The sensitivity functions are plotted in figure 5.

The templates for *nominal stability* are nearly respected (*Templates 1*, *2* and *3*). The maxima of the sensitivity function and of the complementary sensitivity function are equal to 8 dB, which is high but acceptable (4.4 dB of gain margin and 22.8° of phase margin). The maxima of the closed-loop *identified* sensitivity functions (dashed lines) are a little bit higher than the designed ones, so that stability margins of the real system may be lower than expected margins. Bandwidth, linearity and noise shaping templates (*4*, *6* and *9*) are fulfilled, so that the sensor system should respect linearity (THD) and analog to digital conversion resolution requirements (SQNR). Unfortunately *Template 5*, which concerns measurement accuracy, could not be respected (too restrictive). Nevertheless, the system displays good accuracy results. Indeed, as accuracy is equal to the inverse of the sensitivity function $\mathbf{S}$, the $\mathbf{S}$ sensitivity

[2] Design choice imposes that $|G_{d_1}(z^{-1})| \simeq 1$ in the MBW.

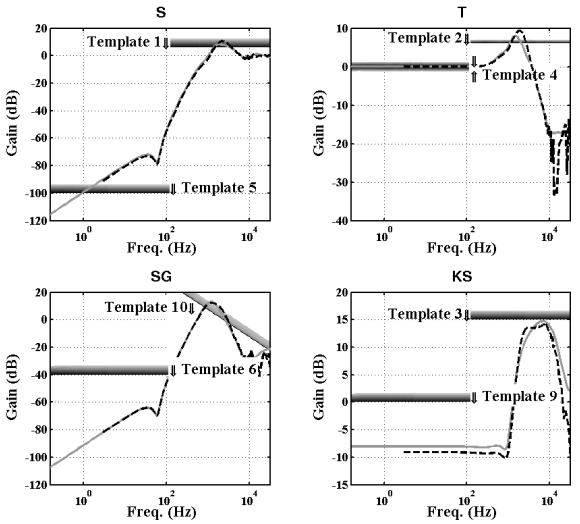

Fig. 5. Templates, sensitivity functions calculated from the identified model in grey lines and sensitivity functions identified on the realistic Simulink® model (with non-linearity, $\Sigma\Delta$ ADC/DAC, ...) in black dashed lines.

plot shows that the sensor accuracy will be theoretically infinite for constant accelerations $\gamma(t)$ (limited by the quantization noise). For low frequency accelerations ($\leq$ 1 Hz), the measurement accuracy will be over 100 dB (55 dB for the specified Measurement Bandwidth). The last template (*Template 10*) concerns *stability robustness* towards parameter variations (damping coefficient). This template is not respected. Further investigations showed that *stability robustness* should be ensured for operating temperatures varying from $3°C$ to $52°C$. Nevertheless, the system has been simulated for operating temperatures of $0°C$ and $85°C$ and in both cases, the system was stable. The resulting sensitivity functions were not modified for frequencies under 122 Hz, showing *(measurement) performance robustness.*

4.2 Sensor performance analysis

The aim of the sensor is to measure and to convert the external acceleration $\gamma(t)$. Several criteria exist in order to characterize sensor performance. Their computations are performed using the spectrum of the measurement output signal $\gamma_m(k)$ (fig. 3a.) for a sine input acceleration $\gamma(t)$ at a given amplitude and frequency (example in fig. 6). Matlab simulations of the complete model forecast excellent results. The *Maximum Signal to Noise Ratio* reaches 100 dB for 3 g acceleration input. The *Smallest detectable acceleration amplitude* equals to $20\mu g$, so that the *Dynamic Range* is over 100 dB, while the *Total Harmonic Distortion* remains under the *quantization noise floor*. So the control loop design fulfils its first aim, which was to reduce nonlinearity effects.

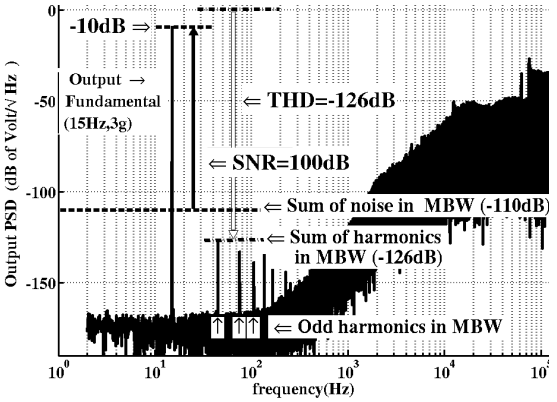

Fig. 6. Example of measurement output ($\gamma_m(t)$) spectrum for an input signal $\gamma(t) = 3gsin(2.\pi.15.t)$

5. REAL SENSOR

A prototype of the presented microsensor has been realized (Condemine *et al.* 2005). The mechanical part area measures around 6 mm^2 while the electronic part measures around 15 mm^2.
The measurement performance of the first prototype is more than promising despite some limitations. Indeed, in order to reduce some additional electronic noise attributed to the test card, the sampling frequencies had to be reduced. Furthermore, the MEMS behaviour is not exactly as expected, so that the feedback actuation voltage V_{fb} had to be reduced. As a consequence, the identified plant's natural frequency is around 400 Hz and its gain equals -4 dB. Nevertheless, the controller design methodology applied to this new system allowed to achieve the following measurement performance (fig. 7 and table 2):
(1) The Analog to Digital conversion resolution is equal to 15 *bits* for a 50 Hz bandwidth (noise floor $E_{rms}(50\ Hz) = -88\ dB$), fig. 7.a.
(2) The proof mass displacement in the measurement bandwidth is lower than the size of an atom for a constant external acceleration (fig. 7.b). For an acceleration input amplitude equal to $\pm 4.5g$, the mass displacement can be estimated (fig. 7.d&f) to be around $4\mathring{A}$ (0.05% of the mass normalized displacement). It can be deduced (fig. 2) that, in most cases, the harmonic distortion will remain under the quantization noise floor. For this prototype, the maximum measurement nonlinearity is expected (starred value in table 2) to be lower than $0.05\%FS$ for any acceleration in the measurement bandwidth and in the dynamic range.
(3) The signal $y_1(t)$ (fig. 7.d&f) can also be considered as the measurement error $\varepsilon_m(t)$ multiplied by the plant gain (fig. 3). Consequently, comparing figures 7.c&d, it can be deduced that the relative measurement error $\varepsilon_m(t)/\gamma(t)$ is arround -50 dB (0.3%) for this $\pm 4.5g$ imposed acceleration.

Table 2. Performance comparison to commercial sensors (From datasheets. Typical values of output noise includes noise from recommended RC-antialiasing filter in case of analog output.)

Company Sensor References	AnalogDevice ADXL320	Applied MEMS SF1500L	MEMS IC MXD7210	VTI SCA320	This study Prototype	Units
Type	Open-loop	Closed-loop	Open-loop	Open-loop	Closed-loop	
Measurement Full Scale	5	3	10	12	10	g
Number of sensing axes	2	1	2	1	1	
Meas. BandWidth (MBW)	50	100	1	400 ± 150	50	Hz
Output Noise in MBW	318	0.5	400	96	60	$\mu g/\sqrt{Hz}$
Meas. Non-Linearity	0.2	0.1	1	1.7	0.05*	$\%FS$
Output type	analog	analog	PWM	analog	digital ($\Sigma\Delta$)	
Supply Voltage	3	$\pm 6\ to \pm\ 15$	5	3	3.3	$Volt$
Power Consumption	1.5	≤ 300	16	10	2.7	mW

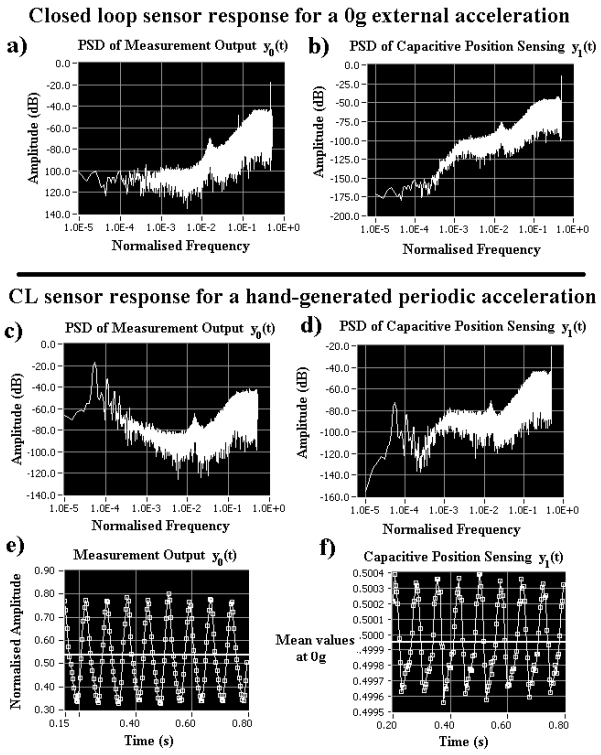

Fig. 7. Measured Results: PSD of measurement output and capacitive position sensing output for a constant acceleration (a&b) and for a $\pm$ 4.5 g hand-generated acceleration (c&d). e&f Corresponding temporal response. Normalizing frequency $f_{norm} = 87.5\ kHz$.

6. CONCLUSION

A control system approach was applied to design a micromachined accelerometer with improved measurement characteristics. In particular, the initial measurement performance specifications have been translated into frequency templates to be fulfilled by the closed-loop system sensitivity functions. The simulation results show that the closed-loop microsystem fulfils its main specifications, while the good real-time results of the first prototypes show the validity of the methodology, despite the fact that the system's behaviour is slightly different compared to the designed one. This methodology is believed to be transposable to other low-pass microsensors.

ACKNOWLEDGEMENT

The authors thank Tronic's Microsystems for sensor design, manufacturing and testing.

REFERENCES

Chau, K.H.L. *et al.* (1996). An integrated force-balanced capacitive accelerometer for low-g applications. *Sensors and Actuators A,* **54**, 472–476.

Condemine, C. *et al.* (2005). a 0.8mA 50Hz 15b SNDR $\Sigma\Delta$ closed-loop 10g accelerometer using an 8^{th}-order digital compensator. *Proc. of the 2005 IEEE Int. Solid-State Circuits Conference, San Fransisco,* **13.6**, 248–249.

Delorme, N., C. Condemine and D. Barbier (2003). Sigma-delta microsystems for read-out and servo control. *Proc. of the SPIE - The Int. Society for Optical Engineering,* **5116**, 270–277.

Doyle, J.C., B.A. Francis and A.R. Tannenbaum (1992). *Feedback Control Theory.* Maxwell Macmillan Intern. Eds.

Handtmann, M. *et al.* (2002). Sensitivity enhancement of MEMS inertial sensors using negative springs and active control. *Sensors and Actuators A,* **97-98**, 153–160.

Kraft, M. (2000). Micromachined inertial sensors: The state of art and a look into the future. *IMC Measurement and Control,* **33(6)**, 164–168.

Landau, I.D. and A. Karimi (1998). Robust digital control using pole placement with sensitivity function shaping method. *Int. Journal of Robust and Nonlinear Control,* **8**, 191–210.

Lemkin, M.A. *et al.* (1997). A 3 axis force balanced accelerometer using a single proof-mass. *Proc. of the 1997 Int. Conference on Solid-State Sensors and Actuators, Chicago,* **2**, 1185–1188.

Norsworthy, S.R., R. Schreier and G.C. Temes (1996). *Delta-Sigma Data Converters: Theory, Design and Simulation.* New York: IEEE Press.

Skogestad, S., I. Postlethwaite (1996). *Multivariable Feedback Control.* John Wiley & Sons.